Robust Hybrid Beamforming in Cooperative Cell-free mmWave MIMO Networks Relying on Imperfect CSI

Meesam Jafri, *Member, IEEE,* Pankaj Kumar, *Student Member, IEEE,* Suraj Srivastava, *Member, IEEE,* Aditya K. Jagannatham, *Senior Member, IEEE,* and Lajos Hanzo, *Life Fellow, IEEE*

***Abstract*—A low-complexity robust cooperative hybrid beamformer is designed for both the downlink and uplink of cell-free millimeter wave (mmWave) multiple-input-multiple-output (MIMO) networks, while considering realistic imperfect channel state information (CSI). To begin with, a second-order cone program (SOCP)-based robust fully-digital beamformer (FDBF) is designed for minimizing the worst-case interference for the downlink of multiple-input-single-output (MISO) systems. Subsequently, we develop a Bayesian learning (BL) framework for determining both the analog and digital components of the hybrid transmit precoder (TPC) from the FDBF. The above designs are subsequently extended to employing eigenvector perturbation theory for constructing the robust TPC for the cell-free mmWave MIMO downlink, where the users have multiple receive antennas (RAs). Furthermore, the multi-dimensional covariance fitting (MCF) framework is harnessed for designing the robust TPC of the corresponding uplink. Finally, the efficiency of the proposed TPC designs is evaluated by simulation results both in terms of their ability to mitigate the multi-user interference (MUI), and improving the spectral efficiency achieved. Additionally, the proposed designs are shown to be computationally efficient and equivalent to a minimum variance hybrid beamformer.**

***Index Terms*—mmWave, cooperative beamforming, cell-free networks, robust beamforming, CSI uncertainty.**

I. Introduction

The increasing need for ultra-high data rates, fuelled by novel applications and the exponential increase in the number of connected devices, has consistently driven the evolution of wireless networks. The existing sub-6 GHz frequency bands are experiencing significant congestion due to limited bandwidth availability. The high-frequency millimeter-wave (mmWave) technology, which operates in the frequency range of $30 - 300$ GHz, has the potential of meeting the ever-increasing demand for high data rates in next-generation (NG) wireless networks [1]–[3]. However, the practical realization of mmWave technology still faces multiple challenges, such as severe signal blockage, high path loss, and hardware complexity, resulting in low received signal [4], [5]. As a remedy, network densification is capable of mitigating these challenges by creating small cells illuminated by distributed access points (APs) [6]. This can potentially reduce the distance between a user and the AP, hence enhancing network coverage and the area spectral efficiency (ASE) quantified in terms of $\mathrm{bit/sec/Hz/m^2}$. However, the reduced mmWave cell size may introduce increased inter-cell interference (ICI), thereby constraining the overall system performance [7]. Furthermore, users located at the cell edge might continue to experience eroded communication quality due to the susceptibility of mmWave beams to blockage.

To address these challenges, the cell-free multiple-input-multiple-output (MIMO) framework has been introduced as a prospective architecture for NG wireless networks [8]–[10]. This approach has emerged as a viable strategy for enhancing the system throughput by surmounting the limitations inherent in the traditional fixed cell arrangement. Through the utilization of multiple cooperative APs for supporting multiple users, the cell-free network improves the available spatial degrees of freedom. This facilitates efficient cooperative transmission and reception, which results in improved performance and judicious rate-fairness.

In addition to its wider bandwidth, the shorter wavelength of mmWave signals offers the advantage of implementing large antenna arrays on compact devices. This MIMO system configuration can deliver the much needed beamforming gain crucial for mmWave networks to counteract the effects of substantial blockages, atmospheric absorption, and penetration losses that typify communication in the mmWave band [11]–[13]. Nevertheless, in a conventional MIMO system employing a fully digital (FD) signal processing architecture, each antenna element necessitates a dedicated radio frequency chain (RFC). The substantial number of

L. Hanzo would like to acknowledge the financial support of the Engineering and Physical Sciences Research Council (EPSRC) projects under grant EP/Y037243/1, EP/W016605/1, EP/X01228X/1, EP/Y026721/1, EP/W032635/1, EP/Y037243/1 and EP/X04047X/1 as well as of the European Research Council's Advanced Fellow Grant QuantCom (Grant No. 789028)

The work of Aditya K. Jagannatham was supported in part by the Qualcomm Innovation Fellowship; in part by the Qualcomm 6G UR Gift; and in part by the Arun Kumar Chair Professorship.

The work of S. Srivastava was supported in part by IIT Jodhpur's Research Grant No. I/RIG/SUS/20240043; in part by Anusandhan National Research Foundation's PM-ECRG/2024/478/ENS; and in part by Telecom Technology Development Fund (TTDF) under Grant TTDF/6G/368.

M. Jafri and A. K. Jagannatham are with the Department of Electrical Engineering, Indian Institute of Technology Kanpur, 208016, India (e-mail: meesam@iitk.ac.in, adityaj@iitk.ac.in.). S. Srivastava is with the Department of Electrical Engineering, Indian Institute of Technology Jodhpur, 342030, India (e-mail: surajsri@iitj.ac.in). P. Kumar and L. Hanzo is with the School of Electronics and Computer Science, University of Southampton, Southampton SO17 1BJ, U.K. (e-mail: pankaj.kumar@soton.ac.uk, lh@ecs.soton.ac.uk)

TABLE I: List of acronyms

MIMO	multiple-input multiple-output
SOCP	Second-order cone program
FDBF	Fully-digital beamformer
MISO	multiple-input-single-output
BL	Bayesian learning
TPC	Transmit precoder
TA	Transmit antenna
RA	Receive antenna
MCF	Multi-dimensional covaraince fitting
MUI	Multi-user interference
RFC	Radio frequency chain
HBF	Hybrid beamformer
BB	baseband
H-RDBF	Hybrid robust downlink beamformer
H-RUBF	Hybrid robust uplink beamformer
DL	downlink
UL	Uplink
UE	User-equipment
T-ARV	Transmit array response vector
R-ARV	Receive ARV
CSI-UA	CSI uncertainty agnostic
RCBF	Robust Capon beamforming
PCSI	Perfect CSI
QoS	Quality of service
AoA	Angle of arrival
AoD	Angle of departure

RFCs required by large antenna arrays results in escalating cost and power consumption. Thus, these factors restrict the viability of the FD signal processing architecture in mmWave MIMO systems [14]–[16]. A promising solution to surmount this challenge involves harnessing a novel hybrid RF baseband (BB) MIMO architecture. This innovative technique utilizes a considerably lower number of RFCs than the total number of antennas. However, the efficient design of the hybrid beamformer (HBF) requires the availability of perfect channel state information (CSI), which is challenging to obtain in practice due to limited feedback and pilot sequence length. If not appropriately addressed, the resultant finite-resolution and outdated CSI may lead to substantial performance erosion in the overall system. Consequently, it becomes imperative to develop a resilient cooperative HBF scheme for cell-free mmWave MIMO networks that incorporates the CSI imperfections. For quick reference, a list of acronyms used in this work is provided in Table I.

A. Related Works

The HBF design has garnered significant attention in recent years as a promising architecture for mmWave MIMO networks. The early contributions were focused on designing the hybrid precoders for single-user scenarios [15], [17]–[20]. As a further development, the authors of [21]–[25] investigated the HBF design for multi-user (MU) mmWave MIMO systems. Liang *et al.* [21] proposed a phased zero-forcing (PZF) low-complexity HBF scheme for MU mmWave MIMO systems, wherein the RF transmit precoder (TPC) is designed by matching the phase of the conjugate transpose of the downlink channel and the BB transmit TPC is obtained via the zero-forcing (ZF) method. Ni and Dong designed the RF combiners for each user based on the principle of equal-gain transmission in order to attain a significant array gain. Subsequently, the BB TPC was derived using the popular block-diagonalization (BD) method for mitigating the multi-user interference (MUI). Khateeb *et al.* [23] proposed a low-complexity iterative method to obtain the HBF weights, which results in significant spectral efficiency gains. This proposed framework exploited the inherent sparsity of the mmWave wireless channel for conceiving an efficient design. Sohrabi *et al.* [24] proposed a heuristic HBF design that approaches the performance of the FD beamformer (FDBF), despite having a limited number of RFCs. Zhan and Dong [25] proposed a successive interference cancellation (SIC)-based HBF design, wherein the ZF method is employed to mitigate the MUI and SIC is used for reducing the intra-user interference.

As a further development, several authors have investigated the HBF design of cooperative mmWave multi-cell networks [26]–[29]. Zhu *et al.* [26] proposed a cooperative HBF design for mmWave multi-cell networks, where they decomposed the analog TPCs and array manifold vectors into Kronecker products of unit-magnitude vectors. Sun *et al.* [27] put forward a regularized ZF-based HBF for both single-stream and multi-stream transmission in cooperative mmWave multi-cell networks. Kim *et al.* [28] proposed HBF schemes for cloud radio access networks, wherein the weighted minimum-mean-square-error (MMSE)-based block coordinate descent (BCD) framework was employed for handling the unit-magnitude constraint of the RF TPC. Fang *et al.* [29] considered joint transmission and base station (BS) silencing approach for designing the HBF schemes. Their proposed framework considered both fully and partially connected hybrid architectures and minimized the sum-power of the BSs.

Several authors explored HBF schemes conceived for mmWave cell-free MIMO networks [8], [30]–[32]. Femenias and Riera [8] considered both the downlink (DL) and uplink (UL) of mmWave cell-free MIMO systems and evaluated the per-user rate of the system. In particular, their RF TPC was obtained based on the second-order statistics of the mmWave wireless channel, whereas the BB TPC was designed by exploiting the small-scale estimated CSI. As a further development, Alonzo *et al.* [30] proposed energy-efficient HBF designs by harnessing the subspace decomposition framework for dividing the FD TPCs into its RF and BB constituents. Feng *et al.* [31] proposed a low-complexity BCD scheme for their HBF design to overcome the challenges of unit-magnitude constraints imposed on the RF TPC, which maximizes the weighted sum rate. Nguyen *et al.* [32] proposed both semi-centralized and decentralized HBF designs for the uplink, where the BB TPC is designed specifically at each access point (AP), and the RF TPC is obtained at the control unit (CU). Furthermore, Jafri *et al.* [33] designed the HBF for both unicast and multicast scenarios by mitigating the MUI in cooperative mmWave cell-free MIMO networks.

The performance of hybrid beamformer critically relies

on having access to channel state information (CSI). Recent research in cell-free MIMO systems has introduced advanced methods for estimating the channels in cell-free networks. However, high dimensional channel estimation in cell-free mmWave MIMO networks is extremely challenging due to the requirement of a high pilot overhead and the limited computing capability of the APs [34]. To address these challenges, several contributions have leveraged the sparse nature of the mmWave channel. Leveraging this sparsity can notably decrease the pilot overhead, while still enhancing the estimation accuracy. Towards this, Zhao *et. al.* [35] proposed an enhanced sparse Bayesian learning (ESBL) procedure for sparse channel estimation in cell-free mmWave networks. The proposed framework first obtains the high-dimensional received signal at each AP, but only a low-dimensional received signal is fed back to the CPU via backhaul links for sparse estimation. The contributions reviewed above design the HBF based on the assumption that perfect CSI is available at each AP. However, obtaining perfect CSI at APs is not feasible in practice due to realistic factors such as channel estimation error, outdated CSI, and quantized feedback [36]. Hence, Palhares *et al.* [37] proposed an MMSE-based robust TPC design relying on imperfect CSI, which minimized the effect of channel estimation errors. As a further advance, Li *et al.* [38] proposed an alternating direction method of multipliers (ADMM) based TPC for cell-free massive MIMO systems. Yu *et al.* [39] proposed a rate-splitting multiple access (RSMA) framework for enhancing the system's throughput in the downlink of cell-free MIMO systems considering the availability of only imperfect channel knowledge. Yao *et al.* [40] conceived robust beamformers for an reconfigurable intelligent surface (RIS)-aided cell-free system for maximizing the worst-case sum rate.

However, the aforementioned treatises primarily concentrated on designing robust FD TPCs for cell-free systems, requiring an excessive number of RFCs. Furthermore, our previous work [33] designed the cooperative HBF for mmWave cell-free MIMO networks by considering the availability of perfect CSI, which is difficult to obtain in practice. Thus, inspired by the aforementioned knowledge gap in the existing literature, we conceive a robust HBF design relying on imperfect CSI for both the DL and UL of cooperative mmWave cell-free systems. Table II presents a bold and explicit contrast to the literature, which is also detailed below.

B. Contribution

This work presents the cooperative robust HBF design of cell-free mmWave MIMO systems in the face of imperfect channel knowledge.

- We commence with the cooperative hybrid robust downlink beamformer (H-RDBF) design of cell-free mmWave systems by considering a single receive antenna (RA) at each user. The pertinent optimization framework is shown to be non-convex, which renders it mathematically challenging. Consequently, a novel two-step framework is developed for addressing this issue. In the first step, the problem is formulated as a second-order cone program (SOCP) for minimizing the worst-case interference to obtain the robust FDBF. Next, a Bayesian learning (BL)-based framework is employed for splitting the FDBF into its RF and BB parts for obtaining the H-RDBF. The key novelty of our work is to derive the robust HBF, in contrast to our previously published work [33], which considered the availability of perfect CSI.
- Subsequently, the H-RDBF design framework is extended to mmWave MIMO scenarios considering multiple RAs at each user. The classic eigenvector perturbation theory is employed for characterizing the ellipsoidal uncertainty and the uncertainty radius. We also demonstrate that the proposed robust TPC vectors are equivalent to the beamformers derived in [33] with the aid of perfect CSI.
- Next, we propose a robust hybrid uplink beamformer (H-RUBF) design for the cell-free mmWave uplink scenario by harnessing a novel multidimensional covariance fitting (MCF) approach that efficiently mitigates the degradation of SINR caused by imperfect CSI.
- Finally, it is shown that the proposed techniques perform similarly to the perfect CSI scenario, demonstrating their improved spectral efficiency and enhanced interference cancellation capability.

C. Notation

Matrices and vectors are represented by boldfaced upper and lowercase letters, respectively, while scalar quantities are denoted by lowercase letters. The conjugate, transpose, Hermitian, and inverse of a matrix $\mathbf{A}$ are denoted by $\mathbf{A}^*$, $\mathbf{A}^T$, $\mathbf{A}^H$, and $\mathbf{A}^{-1}$, respectively. Furthermore, the quantities $\|\mathbf{x}\|_{\mathbf{2}}$ and $\|A\|_F$ denote the l_2-norm and Frobenius of a vector $\mathbf{a}$ and matrix $\mathbf{A}$, respectively, while $\mathbf{Tr}(\mathbf{A})$ is the trace of a matrix $\mathbf{A}$. The quantity $\mathbb{E}[.]$ signifies the expectation operator. Furthermore, $\mathbf{I}$ denotes an identity matrix of suitable size, and $\mathbf{A} \succeq 0$ indicates that the matrix $\mathbf{A}$ belongs to the cone of positive semi-definite (PSD) matrices. A brief list of the main notations is provided in Table III.

II. System Model

Consider a cooperative cell-free mmWave MIMO system relying on N APs, connected to a control unit (CPU), and U user equipment (UEs) relying on the hybrid signal processing architecture illustrated in Fig. 1. Each AP has N_T transmit antennas (TAs) and N_{RF} RFCs, where we have $1 \leq N_{\mathrm{RF}} << N_T$, $\forall n, 1 \leq n \leq N$, and provides service to U UEs with N_u receive antennas (RAs) and U_{RF} RFCs each, $1 \leq U_{\mathrm{RF}} << N_u$, $\forall 1 \leq u \leq U$. The downlink signal $\mathbf{z}_u$ received at the output of the RF receive combiner $\mathbf{W}_{\mathrm{RF},u} \in \mathbb{C}^{N_u \times U_{\mathrm{RF}}}$ of the uth UE can be expressed as

TABLE II: Boldly contrasting our work to the existing literature

	[15]	[21]	[25]	[26]	[29]	[8]	[30]	[31]	[32]	[33]	[37]	[38]	[39]	Proposed Work
mmWave communication	✓	✓	✓	✓	✓	✓	✓	✓	✓	✓				✓
Hybrid architecture	✓	✓	✓	✓	✓	✓	✓	✓	✓	✓				✓
Multi-user		✓	✓	✓	✓	✓	✓	✓	✓	✓	✓	✓	✓	✓
Cooperative beamforming			✓	✓	✓	✓	✓	✓		✓			✓	✓
Downlink	✓	✓	✓		✓	✓	✓	✓		✓			✓	✓
Uplink				✓					✓	✓	✓	✓		✓
Cell-free						✓	✓	✓	✓	✓	✓	✓	✓	✓
Robust FDBF											✓	✓	✓	✓
Joint downlink and uplink														✓
Robust HBF														✓

TABLE III: List of notations

N	Number of APs
N_T	Number of TAs at each AP
N_{RF}	Number of RFCs at each AP
U	Number of UEs
N_u	Number of RAs at each UE
U_{RF}	Number of RFCs at each UE
$\mathbf{G}_{\mathrm{RF},n}$	RF TPC matrix at nth AP
$\mathbf{g}_{\mathrm{BB},u,n}$	BB TPC for uth UE
$\mathbf{H}_{u,n}$	Channel vector between nth AP and uth UE
$\mathbf{W}_{\mathrm{RF},u}$	RF matrix at uth UE
γ_{nk}	Target SINR of UE_{nk}
Q	Size of dictionary matrix
$\mathbf{e}$	CSI error vector
$\mathbf{D}_T$	Dictionary matrix

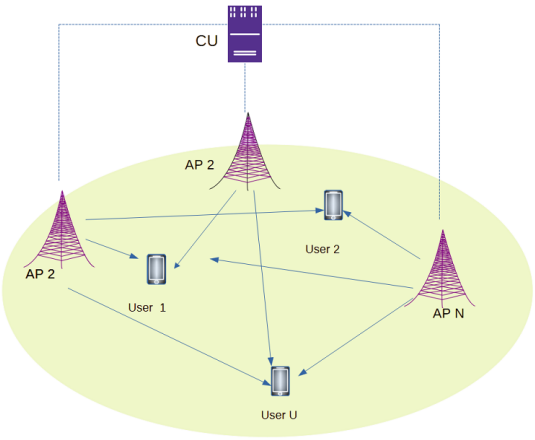

Fig. 1: Cooperative cell-free mmWave MIMO network

$$\mathbf{z}_u = \mathbf{W}_{\mathrm{RF},u}^H \sum_{n=1}^{N} \mathbf{H}_{u,n}\mathbf{G}_{\mathrm{RF},n}\mathbf{g}_{\mathrm{BB},u,n}s_u + \mathbf{W}_{\mathrm{RF},u}^H \sum_{\substack{i=1 \\ i\neq u}}^{U}\sum_{n=1}^{N} \mathbf{H}_{u,n}\mathbf{G}_{\mathrm{RF},n}\mathbf{g}_{\mathrm{BB},i,n}s_i + \tilde{\mathbf{n}}_u, \quad (1)$$

where $\mathbf{g}_{\mathrm{BB},u,n} \in \mathbb{C}^{N_{\mathrm{RF}}\times 1}$ and $\mathbf{G}_{\mathrm{RF},n} \in \mathbb{C}^{N_T\times N_{\mathrm{RF}}}$ denote the BB and RF TPCs at the nth AP for the uth UE, respectively. Furthermore, s_u represents the unit power symbol intended for user u and $\tilde{\mathbf{n}}_u = \mathbf{W}_{\mathrm{RF},u}^H\mathbf{n}_u$ denotes the effective noise vector, where $\mathbf{n}_u \in \mathbb{C}^{N_R\times 1}$ represents the Gaussian noise at UE u with mean zero and variance σ_n^2 of each element. The SINR of the uth user can be expressed as

$$\mathrm{SINR}_u = \frac{\|\mathbf{W}_{\mathrm{RF},u}^H \sum_{n=1}^{N} \mathbf{H}_{u,n}\mathbf{G}_{\mathrm{RF},n}\mathbf{g}_{\mathrm{BB},u,n}\|^2}{\|\mathbf{W}_{\mathrm{RF},u}^H \sum_{\substack{i=1 \\ i\neq u}}^{U}\sum_{n=1}^{N} \mathbf{H}_{u,n}\mathbf{G}_{\mathrm{RF},n}\mathbf{g}_{\mathrm{BB},i,n}\|_2 + \sigma_n^2}. \quad (2)$$

Therefore, the capacity C expression can be formulated as

$$C = \sum_{u=1}^{U} \log_2\left(1 + \mathrm{SINR}_u\right). \quad (3)$$

Upon employing the geometric channel model discussed in [15], [41], the channel matrix $\mathbf{H}_{u,n} \in \mathbb{C}^{N_u\times N_T}$ spanning from the nth AP to uth UE can be expressed as

$$\mathbf{H}_{u,n} = \sqrt{\frac{N_T N_R}{L}} \sum_{l=1}^{L} \alpha_{u,n}^{(l)} \mathbf{a}_R(\phi_{l,u,n}^R)\mathbf{a}_T^H(\phi_{l,u,n}^T), \quad (4)$$

where L denotes the number of multipath components and $\alpha_{u,n}^l$ represents the gain of the lth path between the nth AP and the uth UE. Furthermore, the quantities $\mathbf{a}_T(\phi_l^T) \in \mathbb{C}^{N_T\times 1}$ and $\mathbf{a}_R(\phi_l^R) \in \mathbb{C}^{N_R\times 1}$ represent the transmit array response vector (T-ARV) and receive ARV (R-ARV), respectively, where ϕ_l^T and ϕ_l^R denote the angle of departure (AoD) and angle of arrival (AoA), respectively, corresponding to the lth path spanning from the nth AP to the uth UE. Note that the geometric channel model eminently is suitable for mmWave communication due to its ability to accurately capture the sparse scattering, dominant non-line-of-sight (NLOS) paths, and other characteristics of high-frequency propagation [2], [14], [15]. The mmWave MIMO channel can alternatively be expressed concisely as

$$\mathbf{H}_{u,n} = \mathbf{A}_{R,u,n}\mathbf{H}_{u,n}^{\alpha}\mathbf{A}_{T,u,n}^H,$$

where $\mathbf{A}_R = \left[\mathbf{a}_R(\phi_{1,u,n}^R), \ldots, \mathbf{a}_R(\phi_{L,u,n}^R)\right] \in \mathbb{C}^{N_u\times L}$ and $\mathbf{A}_T = \left[\mathbf{a}_T(\phi_{1,u,n}^T), \ldots, \mathbf{a}_T(\phi_{L,u,n}^T)\right] \in \mathbb{C}^{N_T\times L}$ denote the concatenated receive and transmit array response matrices, respectively, as described in [33]. Furthermore, $\mathbf{H}_{u,n}^{\alpha} = \mathrm{diag}\left(\alpha_{u,n}^{(1)}, \alpha_{u,n}^{(2)}, \ldots, \alpha_{u,n}^{(L)}\right)$ denotes the diagonal matrix of path gains.

To consider the CSI uncertainty, let the concatenated channel spanning from the single antenna user u and all the cooperating APs be modeled as $\mathbf{h}_u = [\mathbf{h}_{u,1}, \mathbf{h}_{u,2}, \ldots, \mathbf{h}_{u,N}] \in \mathbb{C}^{NN_T\times 1}$

$$\mathbf{h}_u = \hat{\mathbf{h}}_u + \mathbf{e}, \quad (5)$$

where $\mathbf{h}_{u,n} \in \mathbb{C}^{N_T \times 1}$ represents the channel vector between nth AP and uth UE. Furthermore, $\hat{\mathbf{h}}_u$ denotes the estimated CSI vector and $\mathbf{e}_u$ represents the CSI error, which is modeled as $\mathbf{e} = \mathbf{Q}_u \mathbf{a}_u$, so that $\|\mathbf{a}\|^2 \leq 1$. Furthermore, $\mathbf{Q}_u$ denotes the square root of the positive semi-definite (PSD) matrix $\mathbf{C}_u$, i.e., $\mathbf{C}_u = \mathbf{Q}_u \mathbf{Q}_u^H$. In the literature, this is represented by a well-known ellipsoidal uncertainty model [42]–[44], which can be defined as

$$\mathcal{E}_u = \left\{ \hat{\mathbf{h}}_u + \mathbf{Q}_u \mathbf{a}_u \middle| \, \|\mathbf{a}_u\|_2 \leq 1 \right\}. \tag{6}$$

Next, we describe the robust hybrid beamformer design of cooperative cell-free mmWave networks considering a single RA at each user.

III. BL-BASED H-RDBF DESIGN FOR CELL-FREE MMWAVE MISO SYSTEMS

This section develops the robust HBF (RHBF) design framework for a multiple-input-single-output (MISO) scenario, wherein each UE is equipped with a single RA. Subsequently, the proposed framework is extended to the MIMO scenario in the later sections. The assumption of imperfect CSI significantly increases the complexity of the downlink beamforming problem compared to [33], where perfect CSI was assumed. In this work, imperfect CSI estimates introduce channel uncertainties, necessitating the development of robust optimization frameworks that account for worst-case performance scenarios. Specifically, we employ ellipsoidal uncertainty models and SOCP to design robust FDBF, which are then decomposed into RF and BB components using a Bayesian learning framework. Let $\mathbf{h}_{u,n} \in \mathbb{C}^{N_T \times 1}$ represent the channel vector between the nth AP and uth UE. The signal $z_u \in \mathbb{C}$ received at the uth UE can be written as

$$\begin{aligned} z_u = &\sum_{n=1}^{N} \mathbf{h}_{u,n}^H \mathbf{G}_{\mathrm{RF,n}} \mathbf{g}_{\mathrm{BB},u,n} s_u \\ &+ \sum_{n=1}^{N} \sum_{\substack{j=1 \\ j \neq u}}^{U} \mathbf{h}_{u,n}^H \mathbf{G}_{\mathrm{RF,n}} \mathbf{g}_{\mathrm{BB},j,n} s_j + \mathbf{n}_u. \end{aligned} \tag{7}$$

Let $\mathbf{g}_{\mathrm{BB},u} \in \mathbb{C}^{NN_{\mathrm{RF}} \times 1}$ denote the concatenated BB TPC vector for the uth user, which is defined as $\mathbf{g}_{\mathrm{BB},u} = \left[\mathbf{g}_{\mathrm{BB},u,1}^T, \mathbf{g}_{\mathrm{BB},u,2}^T, \ldots, \mathbf{g}_{\mathrm{BB},u,N}^T\right]^T$. Similarly, the concatenated channel vector spanning from user u and all the cooperating APs is given as $\mathbf{h}_u = [\mathbf{h}_{u,1}^T, \mathbf{h}_{u,2}^T, \ldots, \mathbf{h}_{u,N}^T]^T \in \mathbb{C}^{NN_T \times 1}$. Therefore, the effective received signal at uth UE can be written as

$$z_u = \mathbf{h}_u^H \mathbf{G}_{\mathrm{RF}} \mathbf{g}_{\mathrm{BB},u} s_u + \sum_{\substack{j=1 \\ j \neq u}}^{U} \mathbf{h}_u^H \mathbf{G}_{\mathrm{RF}} \mathbf{g}_{\mathrm{BB},j} s_j + \mathbf{n}_u, \tag{8}$$

where $\mathbf{G}_{\mathrm{RF}} = \mathrm{blkdiag}\left(\mathbf{G}_{\mathrm{RF},1}, \mathbf{G}_{\mathrm{RF},2}, ...\mathbf{G}_{\mathrm{RF,n}}\right) \in \mathbb{C}^{NN_T \times NN_{\mathrm{RF}}}$ denotes the block-diagonal RF TPC matrix corresponding to the nth AP. Note that the knowledge of perfect CSI is essential for efficient information transmission and HBF design. However, in practice, obtaining perfect CSI is unrealistic due to channel estimation errors, delayed feedback, and quantization errors. To address this challenge, we propose robust HBF schemes for cell-free systems. The optimization problem of minimizing the worst-case MUI in the design of the HBF while satisfying the quality-of-service (QoS) constraints with perfect knowledge of CSI is expressed as

$$\begin{aligned} \min_{\gamma, \mathbf{g}_{\mathrm{BB},1}, \ldots, \mathbf{g}_{\mathrm{BB},U}} \quad & \gamma \\ \text{s.t.} \quad & \mathbf{h}_u^H \mathbf{G}_{\mathrm{RF}} \mathbf{g}_{\mathrm{BB},u} \geq 1, \quad \forall u \\ & \mathbf{h}_u^H \mathbf{G}_{\mathrm{RF}} \mathbf{g}_{\mathrm{BB},j} \leq \gamma, \quad j \neq u \\ & |\mathbf{G}_{\mathrm{RF}}(i,m)| = \frac{1}{\sqrt{N_T}} \quad \forall i, m, \end{aligned} \tag{9}$$

where γ denotes the worst-case MUI. Note that the first and second constraints in (9) represent QoS constraints. Furthermore, the third constraint denotes the constant-magnitude constraint imposed on each entry of the RF TPC, which makes the optimization non-convex and, hence, mathematically intractable. To address these challenges, a two-step procedure can be employed for solving the optimization problem (9). First, we determine the FD-TPC by relaxing the constant-magnitude constraint and then obtain the hybrid TPC by decomposing the FD-TPC via a BL-based framework. Thus, substituting $\mathbf{g}_u = \mathbf{G}_{\mathrm{RF}} \mathbf{g}_{\mathrm{BB},u} \in \mathbb{C}^{NN_T \times 1}$ into (9), the optimization problem can be rewritten as

$$\begin{aligned} \min_{\gamma, \mathbf{g}_1, \ldots, \mathbf{g}_u} \quad & \gamma \\ \text{s.t.} \quad & \mathbf{h}_u^H \mathbf{g}_u \geq 1, \ \forall u \\ & \mathbf{h}_u^H \mathbf{g}_j \leq \gamma, \ j \neq u. \end{aligned} \tag{10}$$

Note that when $\mathbf{g}_j$ belongs to the null-space of the matrix $\mathbf{H}_j = [\mathbf{h}_1, \mathbf{h}_2, \ldots \mathbf{h}_{j-1}, \mathbf{h}_{j+1}, \ldots, \mathbf{h}_u]^H \in \mathbb{C}^{(U-1) \times NN_T}$, i.e. imposing the constraint $\mathbf{h}_u^H \mathbf{g}_j = 0$ for $u \neq j$, one can achieve the ZF solutions subject to the constraint on the number of users, i.e., $U \leq NN_T$. This results in complete interference cancellation, i.e., $\gamma = 0$. This necessitates the design of a robust beamformer that minimizes the worst-case MUI for every channel. Therefore, the optimization problem of designing the robust beamformer that minimizes the worst-case MUI while satisfying the QoS constraints can be formulated as

$$\begin{aligned} \min_{\gamma, \mathbf{g}_1, \ldots, \mathbf{g}_U} \quad & \gamma \\ \text{s.t.} \quad & \mathbf{h}_u^H \mathbf{g}_u \geq 1, \ \forall u \\ & \mathbf{h}_u^H \mathbf{g}_j \leq \gamma, \ j \neq u \\ & \forall \, \mathbf{h}_u \in \mathcal{E}_u, \ \forall u. \end{aligned} \tag{11}$$

Observe that although the above problem is convex, solving it remains computationally challenging due to the presence of an infinite number of constraints pertaining to the ellipsoidal uncertainty region. Interestingly, one can convert these numerous constraints into a finite set of constraints by following the seminal results of [42]. Thus, the optimization problem (11) can be recast as the following convex second-order cone program to jointly design the robust FD-TPC for all the users in the mmWave cell-free system

$$\begin{aligned}\min_{\gamma,\mathbf{g}_1,\ldots,\mathbf{g}_U}\ & \gamma \\ \text{s. t.}\quad & \mathbf{g}_u^H\hat{\mathbf{h}}_u - \left\|\mathbf{Q}_u^H\mathbf{g}_u\right\|_2 \geq 1,\ \forall u \\ & \mathbf{g}_j^H\hat{\mathbf{h}}_u + \left\|\mathbf{Q}_u^H\mathbf{g}_j\right\|_2 \leq \gamma,\ j \neq u. \end{aligned} \tag{12}$$

One can note that the optimization problem above is convex and tractable, hence it can be effectively solved using commonly available tools such as CVX [45]. Note that the optimization problem focuses on minimizing the worst-case MUI, which indirectly regulates the transmit power without explicitly including a power normalization factor. This ensures that the TPCs $\mathbf{g}_{\mathrm{BB},u}$ designed operate within practical power limits. Next, we describe the BL-based HBF design procedure, which decomposes the FD-TPC obtained into its RF and BB constituents.

The state-of-the-art BL method can now be invoked for designing the hybrid TPCs via splitting the FD-TPC attained into its RF and BB constituents, as described in our previously published work [33]. Algorithm 1 presents the step-by-step procedure of the BL-based technique for designing the hybrid TPC.

Algorithm 1: BL-based robust hybrid TPC design

Input: Stacked optimal FD TPC matrix $\mathbf{G}_{\mathrm{opt}}$, dictionary matrix $\mathbf{D}_T$, RFCs NN_{RF}, approximation error variance ψ_e^2, stopping parameters τ and $k_{\max}$;

Initialization: $\hat{\delta}_i^{(0)} = 1,\ \forall 1 \leq i \leq S \rightarrow \hat{\mathbf{\Delta}}^{(0)} = \mathbf{I}_S$. Set counter $k = 0$ and $\mathbf{\Delta}^{(-1)} = \mathbf{0}$;

while $\left(\left\|\hat{\boldsymbol{\delta}}^{(k)} - \hat{\boldsymbol{\delta}}^{(u-1)}\right\|^2 > \epsilon \ \text{and} u < u_{\max}\right)$ **do**

  E-step: Evaluate the *a posteriori* covariance and mean

$$\mathbf{\Delta}^{(k)} = \left(\frac{1}{\psi_e^2}\mathbf{G}_T^H\mathbf{G}_T + \left(\hat{\mathbf{\Delta}}^{(u-1)}\right)^{-1}\right)^{-1}$$

$$\tilde{\mathbf{G}}_{\mathrm{BB}}^{(k)} = \frac{1}{\psi_e^2}\mathbf{\Psi}^{(k)}\mathbf{G}_T^H\mathbf{G}_{\mathrm{opt}}$$

  M-step: Compute the estimate of hyperparameter

  for $i = 1, \ldots, S$

$$\hat{\delta}_i^{(k)} = \mathbf{\Psi}_{(i,i)}^{(k)} + \frac{1}{U}\sum_{j=1}^{U}\left|\tilde{\mathbf{G}}_{\mathrm{BB},n}(i,j)\right|^2$$

  end

end

Output: Obtain $\mathbf{G}_{\mathrm{BB}}^*$ and $\mathbf{G}_{\mathrm{RF}}^*$.

IV. BL-based H-RDBF for cell-free mmWave MIMO systems

This section designs the cooperative robust downlink HBF (H-RDBF) for mmWave cell-free systems considering multiple antennas at each user. Note that [33] considers the availability of perfect knowledge of CSI, which renders the beamformer in cooperative cell-free networks feasible. However, the proposed robust beamformer design in this work is significantly more challenging due to the imperfect channel knowledge. We employed eigenvector perturbation theory to obtain the robust beamformers. Each user estimates the downlink MIMO channel with the aid of the reference signals/pilots, and then feeds back the CSI to the BS using codebook-based channel feedback [46]. However, the channel feedback overhead grows linearly with the number of TAs, a challenge that becomes particularly significant in mmWave cell-free systems. For instance, in a scenario of $N_T = 256$ TAs and $N_R = 64$ RAs, the channel matrix consists of $256 \times 64 = 16384$ complex coefficients. The feedback of these channel weights requires quantization, typically using a codebook having 2^B entries, where B is the number of bits per coefficient. Therefore, using $B = 5$ bits per coefficient would require 81920 bits for all the coefficients. A larger codebook improves the beamforming accuracy but increases the feedback overhead proportionally, hence potentially requiring hundreds of thousands of bits per feedback interval. However, one can exploit the schemes proposed in [47], [48] for low-feedback channel estimation. Furthermore, leveraging the sparse nature of mmWave MIMO channels, where only a few multipath components dominate, compressive sensing techniques effectively reduce the channel dimensionality, hence minimizing feedback requirements [49], [50]. The true CSI of the uth UE with ellipsoidal uncertainty can be written as

$$\mathbf{H}_u = \hat{\mathbf{H}}_u + \mathbf{Q}_u\tilde{\mathbf{A}}_u,$$

where $\tilde{\mathbf{A}}_u = [\tilde{\mathbf{a}}_{u,1}, \tilde{\mathbf{a}}_{u,2}, \ldots, \tilde{\mathbf{a}}_{u,NN_T}]$ and $\|\tilde{\mathbf{a}}_{u,l}\|_2 \leq 1$, $1 \leq l \leq NN_T$, incorporates the CSI error. The matrix $\mathbf{H}_u^H\mathbf{H}_u$, according to the uncertainty model, can be formulated as

$$\begin{aligned}\mathbf{H}_u^H\mathbf{H}_u &= \left(\hat{\mathbf{H}}_u + \mathbf{Q}_u\tilde{\mathbf{A}}_u\right)^H\left(\hat{\mathbf{H}}_u + \mathbf{Q}_u\tilde{\mathbf{A}}_u\right) \\ &= \hat{\mathbf{H}}_u^H\hat{\mathbf{H}}_u + \mathbf{A}_u, \end{aligned} \tag{13}$$

where $\mathbf{A}_u = \hat{\mathbf{H}}_u^H\mathbf{Q}_u\tilde{\mathbf{A}}_u + \tilde{\mathbf{A}}_u^H\mathbf{Q}_u^H\hat{\mathbf{H}}_u + (\mathbf{Q}_u\tilde{\mathbf{A}}_u)^H\mathbf{Q}_u\tilde{\mathbf{A}}_u \in \mathbb{C}^{NN_T \times NN_T}$ denotes the effective uncertainty matrix for user u. Next, we employ the eigenvector perturbation theory (EPT) of [51] to incorporate the CSI uncertainty in the principal eigenvector $\mathbf{v}_{u,1}$ of the matrix $\mathbf{H}_u^H\mathbf{H}_u$ for the design of the robust TPC for cooperative mmWave MIMO cell-free systems, as shown next.

Lemma 1 : Let $\hat{\mathbf{v}}_{u,1}$ denotes the eigenvector of $\hat{\mathbf{H}}_u^H\hat{\mathbf{H}}_u$. The perturbed principle eigenvector $\mathbf{v}_{u,1}$ of $\mathbf{H}_u^H\mathbf{H}_u$ can be formulated as

$$\mathbf{v}_{u,1} = \hat{\mathbf{v}}_{u,1} + \sum_{i=2}^{NN_T}\frac{\rho_{u,i1}\hat{\mathbf{v}}_{u,i}}{(\hat{\lambda}_{u,1} - \hat{\lambda}_{u,i})} \tag{14}$$

where $\rho_{u,ij} = \hat{\mathbf{v}}_{u,i}^H\mathbf{A}_u\hat{\mathbf{v}}_{u,j}$ and $\hat{\lambda}_{u,i} = \hat{\sigma}_{u,i}^2$. Furthermore, $\hat{\sigma}_{u,i}$ represents the ith singular value of the matrix $\hat{\mathbf{H}}_u$.

Proof : Shown in Appendix A.

Thus, from the given result, we have

$$\mathbf{v}_{u,1} = \hat{\mathbf{v}}_{u,1} + \mathbf{J}_u\boldsymbol{\rho}_u, \tag{15}$$

where

$$\boldsymbol{\rho}_u = [\rho'_{u,21}, \rho'_{u,31}, \ldots, \rho'_{u,NN_T1}]^T \in \mathbb{C}^{(NN_T-1)\times 1},$$

$$\rho'_{u,l1} = \rho_{u,l1}/(\hat{\lambda}_{u,1} - \hat{\lambda}_{u,l}),$$

$$\mathbf{J}_u = [\hat{\mathbf{v}}_{u,2}, \hat{\mathbf{v}}_{u,3}, \ldots, \hat{\mathbf{v}}_{u,NN_T}] \in \mathbb{C}^{NN_T\times(NN_T-1)}.$$

Next, in Lemma 2, we characterize the magnitude $\|\boldsymbol{\rho}_u\|_2$ of the perturbation vector $\boldsymbol{\rho}_u$.

Lemma 2: The norm of the vector $\boldsymbol{\rho}_u$, associated with the eigenvector $\mathbf{v}_{u,1}$ corresponding to the largest eigenvalue of the matrix $\mathbf{H}_u$, is upper bounded as

$$\|\boldsymbol{\rho}_u\|_2 \leq \underbrace{\left(\frac{\tilde{\sigma}_u}{\hat{\lambda}_{u,1} - \hat{\lambda}_{u,2}}\right)}_{\epsilon_{\rho_u}}, \tag{16}$$

where $\tilde{\sigma}_u$ represents the dominant singular value of $\mathbf{A}_u$.

Proof : Shown in Appendix B.

Therefore, the optimal robust TPC $\tilde{\mathbf{g}}_1$ for the first UE can be designed by solving the following relaxed optimization problem

$$\begin{aligned} \min_{\tilde{\mathbf{g}}_1} \quad & \|\tilde{\mathbf{g}}_1\|_2 \\ \text{s.t.} \quad & \min_{\|\boldsymbol{\rho}_1\|_2 \leq \epsilon_{\rho_1}} \tilde{\mathbf{g}}_1^H(\hat{\mathbf{v}}_{1,1} + \mathbf{J}_1\boldsymbol{\rho}_1) \geq 1, \end{aligned} \tag{17}$$

where the quantity $\mathbf{A}_1$ represents the uncertainty matrix associated with UE 1. Upon simplifying the constraint, the robust TPC design problem can be recast as the SOCP shown below

$$\begin{aligned} \min_{\tilde{\mathbf{g}}_1} \quad & \|\tilde{\mathbf{g}}_1\|_2 \\ \text{s.t.} \quad & \tilde{\mathbf{g}}_1^H\hat{\mathbf{v}}_{1,1} - \epsilon_{\rho_1}\left\|\mathbf{J}_1^H\tilde{\mathbf{g}}_1\right\|_2 \geq 1. \end{aligned} \tag{18}$$

Note that the robust TPCs obtained as the solution to the above optimization problem are equivalent to the optimal successive minimum variance hybrid beamformer (OSHB) TPC [33], except for a scaling factor. The proof of this is provided next.

Theorem 1 : The optimal beamformer, denoted as $\tilde{\mathbf{g}}_1^*$, in the beamformer design problem (18) is proportional to the estimate of the vector $\hat{\mathbf{v}}_{1,1}$ as $\tilde{\mathbf{g}}_1^* = \kappa\hat{\mathbf{v}}_{1,1}$., where κ denotes the constant of proportionality chosen suitably.

Proof : Shown in Appendix C.

Therefore, the optimal TPC $\tilde{\mathbf{g}}_1^*$ corresponding to UE 1 can be determined by performing the singular value decomposition (SVD) of the matrix $\hat{\mathbf{H}}_1$. In general, the uth UE will experience interference from the $u-1$ UEs scheduled before. The interference from the previously scheduled users at the uth user can be minimized by employing the OSHB scheme described in [33]. Towards this, let $\tilde{\mathbf{g}}_u^*$ and $\mathbf{w}_u$ denote the optimal TPCs and receive combiners (RCs) for the uth UE. Employing the framework in [33], the TPCs and RCs designed for interference cancellation are determined as

$$\tilde{\mathbf{g}}_u^* = \hat{\mathbf{M}}_{u-1}^{\perp}\tilde{\boldsymbol{\nu}}_u^* \;\text{ and }\; \mathbf{w}_u^* = (\mathbf{R}_{\boldsymbol{\upsilon}_u}^{-(1/2)})^H\tilde{\mathbf{w}}_u^*,$$

respectively, where $\tilde{\boldsymbol{\nu}}_u^*$ and $\tilde{\mathbf{w}}_u^*$ represent the dominant right and left singular vectors, respectively, of the matrix $\mathbf{R}_{\upsilon_u}^{-(1/2)}\hat{\mathbf{H}}_u\hat{\mathbf{M}}_{u-1}^{\perp}$. Furthermore, $\mathbf{R}_{\upsilon_u}$ represents the covariance matrix of the quantity $\boldsymbol{\upsilon}_u = \sum_{i=1}^{u-1}\hat{\mathbf{H}}_u\hat{\mathbf{M}}_{u-1}^{\perp}\boldsymbol{\nu}_i s_i + \tilde{\mathbf{n}}_u$, and it is given as

$$\begin{aligned} \mathbf{R}_{\upsilon_u} &= \sum_{i=1}^{u-1}\hat{\mathbf{H}}_u\mathbf{g}_i\left(\mathbb{E}\left[|s_i|^2\right]\right)\mathbf{g}_i^H\hat{\mathbf{H}}_u^H + \mathbb{E}\left[\mathbf{n}_u\mathbf{n}_u^H\right] \\ &= \sum_{i=1}^{u-1}\hat{\mathbf{H}}_u\left(\hat{\mathbf{M}}_{i-1}^{\perp}\boldsymbol{\nu}_i\boldsymbol{\nu}_i^H\left(\hat{\mathbf{M}}_{i-1}^{\perp}\right)^H\right)\hat{\mathbf{H}}_u^H + \sigma_n^2. \end{aligned} \tag{19}$$

The matrix $\hat{\mathbf{M}}_{u-1}^{\perp}$, which denotes the estimates of $\mathbf{M}_{u-1}^{\perp}$, represents the basis orthonormal to the null space of the matrix $\hat{\mathbf{M}}_{u-1} \in \mathbb{C}^{NN_T\times(NN_T-u+1)}$

$$\hat{\mathbf{M}}_{u-1} = \left[\left(\mathbf{w}_1^H\hat{\mathbf{H}}_1\right)^T, \ldots, \left(\mathbf{w}_{u-1}^H\hat{\mathbf{H}}_{u-1}\right)^T\right]^T. \tag{20}$$

Once again, one can now invoke the BL-based framework as explained in Section III to obtain the RF and BB TPC/RC. Next, we describe the robust hybrid beamformer designed for the uplink of cell-free mmWave MIMO networks.

V. Hybrid robust uplink hybrid beamforming (H-RUBF)

This section develops our robust cooperative hybrid TPC design of the mmWave cell-free uplink for U users and N APs. For the uplink scenario, the assumption of imperfect CSI introduces additional challenges in mitigating the degradation of the signal-to-interference-plus-noise ratio (SINR) caused by channel estimation errors. In contrast to the uplink beamforming framework in [33], which assumes accurate channel knowledge, this work employs a MCF framework to design H-RUBF. The nth AP has N_T RAs and N_{RF} RFCs, whereas the uth UE is equipped with N_u TAs and U_{RF} RFCs. The uplink signal $\mathbf{y} \in \mathbb{C}^{NN_T\times 1}$ received by all the APs can be expressed as

$$\mathbf{z} = \sum_{u=1}^{U}\tilde{\mathbf{H}}_u\mathbf{v}_u x_u + \mathbf{n} = \sum_{u=1}^{U}\tilde{\mathbf{f}}_u x_u + \mathbf{n}, \tag{21}$$

where $\tilde{\mathbf{H}}_u = \left[\tilde{\mathbf{H}}_{u,1}^H, \tilde{\mathbf{H}}_{u,2}^H, \ldots, \tilde{\mathbf{H}}_{u,N}^H\right]^H \in \mathbb{C}^{NN_T\times N_u}$ and $\mathbf{v}_u$ represent the concatenated channel matrix of user u at the CU and the dominant right singular vector of the matrix $\tilde{\mathbf{H}}_u$, respectively. Note that the CU estimates the channel of all the UEs, which corresponds to the matrix. Subsequently, the CU utilizes this information for calculating the optimal transmit beamformer weights, which are then fed back to the users. The CU feeds back the beamforming vectors to the users either by relying on quantized feedback. For example, if the codebook contains 2^B distinct beamforming vectors, then B bits are needed to represent each beamforming vector. A large codebook enhances the beamforming gain but requires a high number of bits, which in turn increases the overhead. Furthermore, the

optimal receive beamformer $\tilde{\mathbf{w}}_u \in \mathbb{C}^{NN_T \times 1}$ can be obtained as the minimum variance distortionless response (MVDR) beamformer formulated as $\mathbf{C}_z^{-1}\tilde{\mathbf{f}}_u / \tilde{\mathbf{f}}_u^H \mathbf{C}_z^{-1} \tilde{\mathbf{f}}_u$, where we have $\mathbf{C}_z = \sum_{u=1}^{U} \tilde{\mathbf{f}}_u \tilde{\mathbf{f}}_u^H + \sigma_\eta^2 \mathbf{I}_{NN_T}$ and $\tilde{\mathbf{f}}_u = \tilde{\mathbf{H}}_u \mathbf{v}_u$. Let $\mathbf{C}_u \in \mathbb{C}^{NN_T \times NN_T}$ denote a symmetric PSD matrix that models the CSI uncertainty in the vectors $\check{\mathbf{f}}_u, \forall u$. Therefore, the estimates, $\check{\mathbf{f}}_u$, $1 \le u \le U$, in the presence of CSI errors can be modeled as falling within an uncertainty ellipsoid given by $\mathcal{E}_u = \{\tilde{\mathbf{f}}_u | (\tilde{\mathbf{f}}_u - \check{\mathbf{f}}_u)^H \mathbf{P}_u^{-1} (\tilde{\mathbf{f}}_u - \check{\mathbf{f}}_u) \le 1\}$.

Let $\tilde{\mathbf{F}} = [\tilde{\mathbf{f}}_1, \tilde{\mathbf{f}}_2, \ldots, \tilde{\mathbf{f}}_U] \in \mathbb{C}^{NN_T \times U}$ represent the concatenated beamformer matrix. Note that one can formulate an MCF problem by employing the beamformers $\check{\mathbf{F}} = [\check{\mathbf{f}}_1, \check{\mathbf{f}}_2, \ldots, \check{\mathbf{f}}_u]$, CSI error ellipsoids $\mathcal{E}_u$, $1 \le u \le U$, and the covariance matrix $\mathbf{C}_z$ to determine the robust beamformer. The MCF framework evaluates the maximum likelihood estimate of the beamformers, while taking into account the constraints based on the uncertainty ellipsoids and the covariance matrix. Subsequently, the robust beamformers found closely approximate the actual ones, hence reducing the SINR erosion attributed to the imperfect CSI. Therefore, the MCF optimization problem of obtaining the robust uplink beamformer matrix $\check{\mathbf{F}}^*$ can be formulated as

$$\begin{aligned} \max_{\tilde{\mathbf{F}}, \tilde{\sigma}^2 \ge 0} \quad & \log \left| \tilde{\mathbf{F}} \tilde{\mathbf{F}}^H + \tilde{\sigma}^2 \mathbf{I}_{NN_T} \right| \\ \text{s.t.} \quad & \hat{\mathbf{C}}_y \succeq \tilde{\mathbf{F}} \tilde{\mathbf{F}}^H + \tilde{\sigma}^2 \mathbf{I}_{NN_T} \\ & (\tilde{\mathbf{f}}_u - \check{\mathbf{f}}_u)^H \mathbf{P}_u^{-1} (\tilde{\mathbf{f}}_u - \check{\mathbf{f}}_u) \le 1, \ 1 \le u \le U. \end{aligned} \quad (22)$$

One can approximate the above optimization problem of designing the robust uplink beamformer by the following convex problem [52]

$$\begin{aligned} \max_{\tilde{\mathbf{F}}, \tilde{\sigma}^2 \ge 0} \quad & 2\Re\Big\{ \mathrm{Tr}\left\{ \hat{\mathbf{F}}^H \mathbf{C}_{y,0}^{-1} \tilde{\mathbf{F}} \right\} \Big\} + \tilde{\sigma}^2 \mathrm{Tr}\big\{ \mathbf{C}_{y,0}^{-1} \big\} \\ \text{s.t.} \quad & \begin{bmatrix} \hat{\mathbf{C}}_y - \tilde{\sigma}^2 \mathbf{I}_{NN_T} & \tilde{\mathbf{F}} \\ \tilde{\mathbf{F}}^H & \mathbf{I}_u \end{bmatrix} \succeq 0 \\ & (\tilde{\mathbf{f}}_u - \check{\mathbf{f}}_u)^H \mathbf{P}_u^{-1} (\tilde{\mathbf{f}}_u - \check{\mathbf{f}}_u) \le 1, \ 1 \le u \le U, \end{aligned} \quad (23)$$

where we have $\mathbf{C}_{y,0} = \check{\mathbf{F}} \check{\mathbf{F}}^H + \sigma_0^2 \mathbf{I}_{NN_T}$, and σ_0^2 represents the initial estimate of the noise variance. Furthermore, it is interesting to note that the optimization problem (23) is convex in nature, hence easily solvable using widely available tools, such as [45].

Next, we summarize the complexity analysis of H-RDBF and H-RUBF design schemes. Note that the optimization problem in (12) can be efficiently solved using second-order cone programming (SOCP) at a complexity order of $\mathcal{O}\left((UNN_T)^3\right)$, while the optimization problem in (23) can be efficiently solved using SOCP at a complexity of $\mathcal{O}\left((NN_T)^3 + (UNN_T)^2\right)$ [52] for designing the beamformers of all the UEs.

VI. Simulation results

This section provides our simulation results for characterizing the performance of the proposed robust hybrid beamformer schemes in the presence of imperfect CSI for both DL and UL scenarios. In our simulations, we consider a network comprised of $N = \{2, 4\}$ APs and $U = \{4, 8\}$ users that are uniformly distributed in a square area of size 200×200 m^2. The inter-AP distance is 40m. Each AP and user has $N_T = \{32, 64\}$ TAs and $N_u = \{4, 8\}$ RAs, respectively. The mmWave MIMO channel $\mathbf{H}_{u,m}$ corresponding to uth user and nth AP has $L = 6$ multipath components, and the multipath gains $\beta_{u,m}^l$ are generated as $\mathcal{CN}(0, 1)$. It is assumed that the impact of large-scale fading has been fully mitigated through effective power control at each APs. Consequently, this study focuses exclusively on the influence of small-scale fading, consistent with the approach adopted in [26], [53], [54]. Note that the range of error radius ϵ spans from 0.5 to 1.4. The value of $\epsilon = 0$ corresponds to the perfect CSI scenario, while large values of ϵ indicate large error in the CSI. For our BL-based TPC/RC design, the stopping parameters are set to $k_{\max} = 50$ and $\tau = 10^{-6}$. To model the ellipsoid CSI errors, we consider $\mathbf{C}_u = \epsilon^2 \mathbf{I}_{NN_T}, 1 \le u \le U$ for both DL and UL systems. We assume that all transmitters have the same transmit power P, and the signal-to-noise ratio (SNR) is defined as $\frac{P}{\sigma_n^2}$. Table IV shows the detailed parameters considered in our simulations.

TABLE IV: Simulation parameters of System-I and System-II profiles of a cooperative cell-free mmWave MIMO system

Parameter	System-I	System-II
# of APs (N)	2	4
# of users (U)	4	8
# of TAs (N_T)	32	64
# of RAs (N_u)	4	8
# of RFCs at APs (N_{RF})	4	8
# of RFCs at users (N_{RF})	2	4

A. Robust downlink hybrid beamforming

Fig. 2a plots the capacity versus the error radius for the DL of the cell-free mmWave MISO System-I and System-II of Table IV. The figure illustrates that the worst-case MISO RDBF design approaches the performance of the idealized system having perfect CSI (PCSI). Furthermore, the proposed scheme performs better than the CSI uncertainty agnostic (UA) beamformer. This is due to the fact that the CSI-UA scheme fails to incorporate the uncertainty in the channel matrix, while designing the beamformer. Fig. 2b compares the capacity versus the signal-to-noise ratio (SNR) of the proposed MISO RDBF scheme to that of the perfect CSI and CSI-UA beamformers where the latter ignores the CSI uncertainty while designing the TPCs. Observe that the performance of RDBF approaches that of the perfect CSI scenario, demonstrating the efficacy of the proposed robust TPC schemes. Furthermore, one can note that the BL-based hybrid RDBF having notably fewer RFCs ($N_{\mathrm{RF}} = 4$) and ($N_{\mathrm{RF}} = 8$) for System-I and System-II, respectively, performs similarly to that of the FDBF with ($N_{\mathrm{RF}} = 32$) and ($N_{\mathrm{RF}} = 6$) for System-I and System-II, respectively. This is due to the fact that the mmWave MIMO channel has a substantially reduced number of multipath components, a

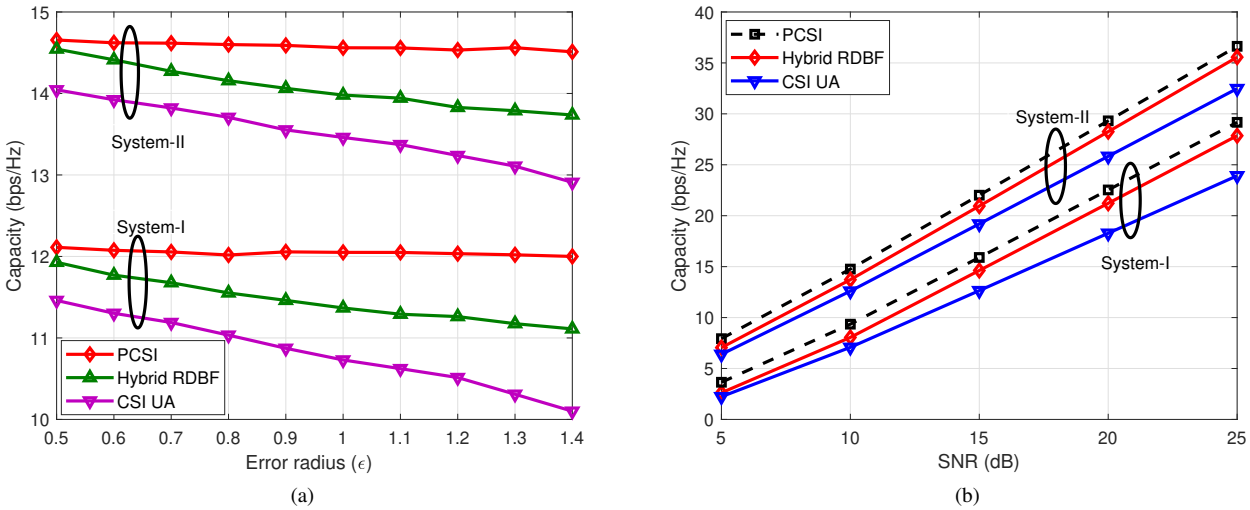

Fig. 2: MISO downlink considering System-I and System-II parameters: (a) Capacity versus error radius (ϵ) for SNR $=$ 10dB. (b) Capacity versus SNR for error radius $\epsilon = 0.6$.

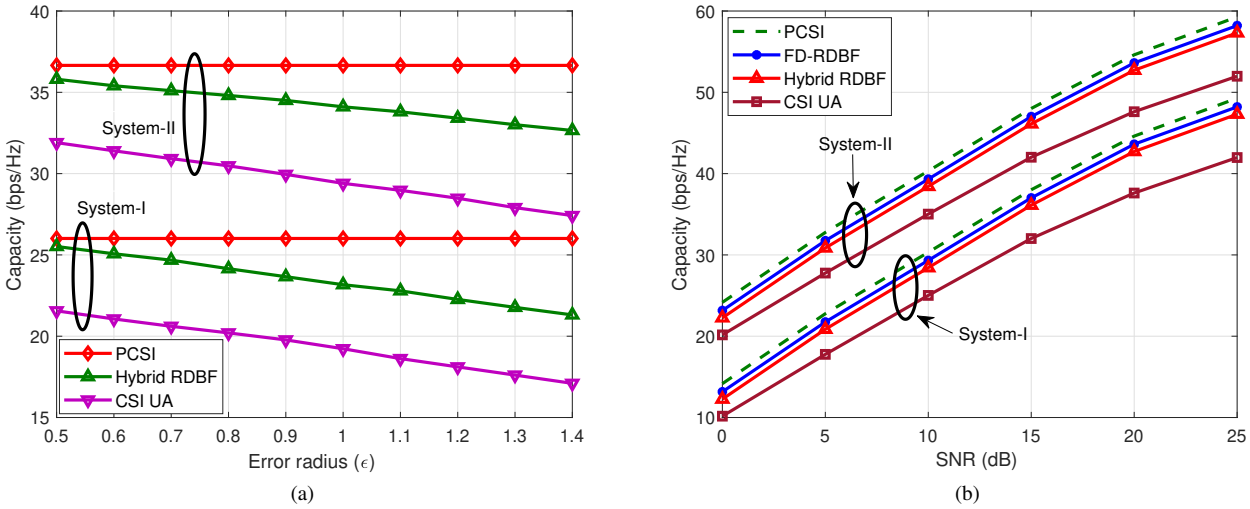

Fig. 3: MIMO downlink performance considering System-I and System-II parameters: (a) Capacity versus error radius (ϵ) for SNR $=$ 10dB. (b) Capacity versus SNR for error radius $\epsilon = 0.6$.

characteristic beneficially exploited by our BL-based hybrid transceiver design. Consequently, a tight approximation of the ideal FDBF can be achieved using only a small number of T-ARVs.

Next, we consider the performance of our robust TPC design conceived for a MIMO downlink scenario in cell-free mmWave networks. Once again, Fig. 3a illustrates the performance of the proposed RDBF schemes along with those of the other schemes for different values of the uncertainty error radius and $SNR = 10$dB. Observe that the capacity of the proposed RDBF scheme decreases upon increasing the CSI uncertainty error radius ϵ. However, the proposed RDBF design still achieves a performance similar to that of the [33], when perfect CSI is available at the CU. Fig. 3b plots the capacity versus SNR of the proposed scheme along with that of other scenarios having an error radius of $\epsilon = 1$ for System-I and System-II. It is interesting to note that an increase in the number of TAs at each AP leads to a capacity enhancement. This can be attributed to the fact that the proposed BL-based hybrid design is capable of efficiently exploiting the resultant enhanced array gain.

The capacity versus the number of APs in our cell-free mmWave MIMO DL system is investigated in Fig. 4. It is evident from the figure that with the increase in the number of APs, the capacity increases. This indicates that harnessing a large number of APs in cell-free MIMO DL systems has

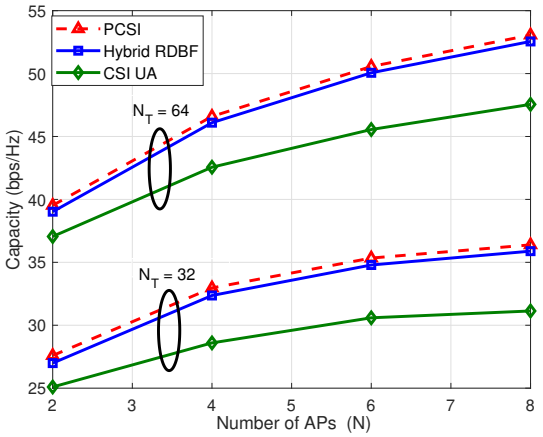

Fig. 4: MIMO downlink capacity versus number of APs for SNR $= 10$dB, $\epsilon = 0.6$ and $U = 6$.

the potential of significantly improving the capacity. Once again, an increase in the number of TAs at each AP enhances the capacity of the system.

B. Robust uplink hybrid beamforming

Fig. 5a characterizes the capacity versus the error radius of the proposed robust beamformer in the uplink of our mmWave cell-free MIMO system. Observe that the MCF technique-based RUBF design performs similarly to the perfect CSI scenario. Furthermore, there is a significant performance gap between the MCF-based RUBF and the robust Capon beamformer (RCBF) [43] at high SNRs. This is due to the better interference cancellation capability of the MCF technique. Fig. 5b illustrates the capacity versus SNR plot of the cell-free uplink for $\epsilon = 0.6$. It can be seen that the performance of the BL-based hybrid RUBF is close to the idealized scenario associated with perfect CSI, and also closely matches the performance of the ideal FD design.

VII. Summary and Conclusions

Robust cooperative hybrid beamformers and combiners were designed for the DL and UL of mmWave cell-free networks. Initially, a novel two-step framework was developed for obtaining the low-complexity robust hybrid beamformer considering single-antenna users. A robust FD beamformer was obtained in the first step, which minimizes the worst-case interference in the presence of CSI uncertainty. Next, a BL-based hybrid TPC design framework was employed to factorize the FD TPC into its RF and baseband TPCs. Subsequently, eigenvector perturbation theory was employed to design robust hybrid TPCs for the cell-free mmWave MIMO downlink, while an MCF-based cooperative robust hybrid beamformer was designed for the uplink. The proposed cooperative robust hybrid TPC design techniques exhibit a notable performance enhancement in cell-free mmWave MIMO networks. It was also seen that the H-RDBF results in a closed-form solution and is equivalent to the successive minimum variance hybrid beamformer. Furthermore, the proposed robust HBF designs have a reduced complexity and the capability to accommodate more users simultaneously compared to other approaches. This makes them highly appropriate for real-world deployment in cell-free mmWave MIMO networks.

Appendix A
Lemma 1:

Proof: The imperfect channel of the uth UE can be expressed as $\mathbf{H}_u^H\mathbf{H}_u = \hat{\mathbf{H}}_u^H\hat{\mathbf{H}}_u + \epsilon\mathbf{A}_u$, where $\epsilon\mathbf{A}_u$ denotes the uncertainty in the CSI. One can observe that as $\epsilon \to 0$, we have $\hat{\mathbf{H}}_u^H\hat{\mathbf{H}}_u \to \mathbf{H}_u^H\mathbf{H}_u$.

Let $\hat{\lambda}_{u,i}$ and $\lambda_{u,i}$, $1 \le i \le NN_T$, denote the eigenvalues of the matrix $\hat{\mathbf{H}}_u^H\hat{\mathbf{H}}_u$ and $\mathbf{H}_u^H\mathbf{H}_u$, respectively. Following the EPT, the true dominant eigenvalue $\lambda_{u,i}$, $1 \le i \le NN_T$ can be expressed as

$$\lambda_{u,1} = \hat{\lambda}_{u,1} + x_{u,1}\epsilon + x_{u,1}\epsilon^2 + \cdots, \tag{24}$$

where $x_{u,i}$ represents the error factor due to the matrix $\mathbf{A}_u$. Once again, note that as $\epsilon \to 0$, the eigenvalue obeys $\hat{\lambda}_{u,1} \to \lambda_{u,1}$ and $\left|\hat{\lambda}_{u,1} - \lambda_{u,1}\right| = O(\epsilon)$. Since $(\mathbf{H}_u^H\mathbf{H}_u)\mathbf{v}_{u,1} = \lambda_{u,1}\mathbf{v}_{u,1}$, one can also express the principal eigenvector as the convergent power series [51],

$$\mathbf{v}_{u,1} = \hat{\mathbf{v}}_{u,1} + \epsilon\mathbf{b}_{u,1} + \epsilon^2\mathbf{b}_{u,2} + \cdots, \tag{25}$$

where $\mathbf{b}_{u,i}$ represents the error vector due to the matrix $\mathbf{A}_u$. Note that the eigenvectors $\{\hat{\mathbf{v}}_{u,i}\}_{i=1}^{NN_T}$ form a basis for the NN_T-dimensional complex space, therefore, each of the vector $\mathbf{b}_{u,i}$ can be expressed as the span of the basis vectors $\{\hat{\mathbf{v}}_{u,i}\}_{i=1}^{NN_T}$ as

$$\mathbf{b}_{u,i} = \sum_{j=1}^{NN_T} \omega_{u,ji}\hat{\mathbf{v}}_{u,j}, \tag{26}$$

where $\omega_{u,ji} \in \mathbb{R}$ denotes the real scalar quantities. Next, substituting the value of $\mathbf{b}_{u,i}$ into (25), the true principal eigenvector $\mathbf{v}_{u,1}$ can be rewritten as

$$\mathbf{v}_{u,1} = \hat{\mathbf{v}}_{u,1} + \epsilon\sum_{j=1}^{NN_T} \omega_{u,j1}\hat{\mathbf{v}}_{u,j} + \epsilon^2\sum_{j=1}^{NN_T} \omega_{u,j2}\hat{\mathbf{v}}_{u,j} + \cdots. \tag{27}$$

The vector $\mathbf{v}_{u,1}$ can be further rewritten as

$$\mathbf{v}_{u,1} = (1 + \epsilon\omega_{u,11} + \epsilon^2\omega_{u,12} + \cdots)\hat{\mathbf{v}}_{u,1} + (\epsilon\omega_{u,21} + \epsilon^2\omega_{u,22} + \cdots)\hat{\mathbf{v}}_{u,2} + \cdots + (\epsilon\omega_{u,NN_T1} + \epsilon^2\omega_{u,NN_T2} + \cdots)\hat{\mathbf{v}}_{u,NN_T}. \tag{28}$$

Subsequently, one can obtain the relationship between the true and the perturbed principal eigenvectors after normalizing the expression in (28) as

$$\mathbf{v}_{u,1} = \hat{\mathbf{v}}_{u,1} + (\epsilon t_{u,21} + \epsilon^2 t_{u,22} + \cdots)\hat{\mathbf{v}}_{u,2} + \cdots + (\epsilon t_{u,NN_T1} + \epsilon^2 t_{u,NN_T2} + \cdots)\hat{\mathbf{v}}_{u,NN_T}, \tag{29}$$

where $t_{u,ji} \in \mathbb{R}$ represents the scalars quantities. Therefore, the first-order perturbed principal eigenvector and eigenvalue can be determined as

$$\mathbf{v}_{u,1} = \hat{\mathbf{v}}_{u,1} + \epsilon\sum_{i=2}^{NN_T} t_{u,i1}\hat{\mathbf{v}}_{u,i}, \tag{30}$$

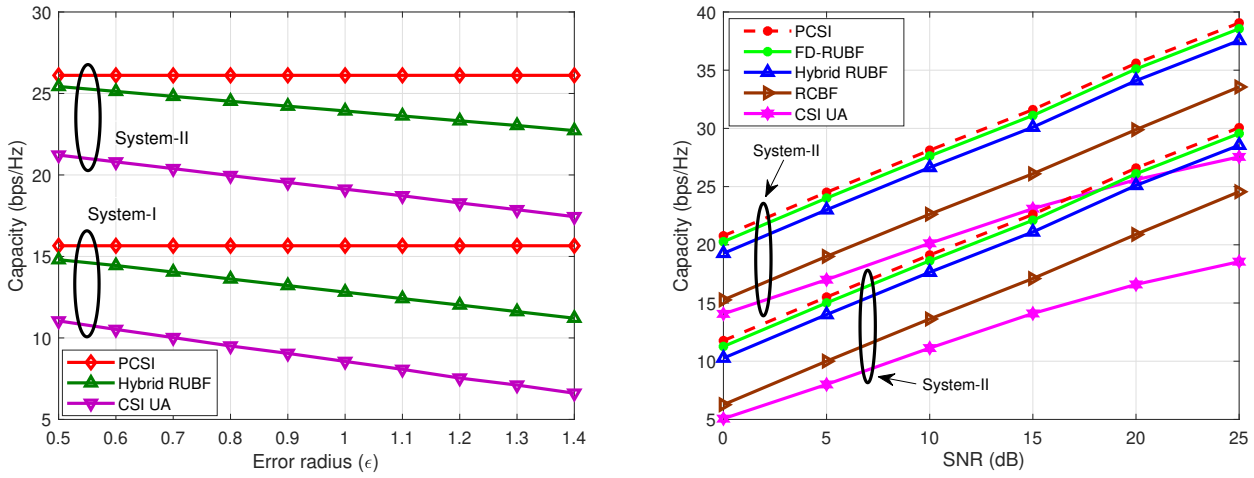

Fig. 5: MIMO Uplink performance considering System-I and System-II parameters: (a) Capacity versus error radius (ϵ) for SNR $= 10$dB. (b) Capacity versus SNR for error radius $\epsilon = 0.6$.

$$\lambda_{u,1} = \hat{\lambda}_{u,1} + x_{u,1}\epsilon,$$

respectively. Thus, one can reformulate the expression for $(\mathbf{H}_u^H\mathbf{H}_u)\mathbf{v}_{u,1} = \lambda_{u,1}\mathbf{v}_{u,1}$ as

$$\begin{aligned}&(\hat{\mathbf{H}}_u^H\hat{\mathbf{H}}_u + \epsilon\mathbf{A}_u)\left(\hat{\mathbf{v}}_{u,1} + \epsilon\sum_{i=2}^{NN_T} t_{u,i1}\hat{\mathbf{v}}_{u,i}\right)\\ &= (\hat{\lambda}_{u,1} + x_{u,1}\epsilon)\left(\hat{\mathbf{v}}_{u,1} + \epsilon\sum_{i=2}^{NN_T} t_{u,i1}\hat{\mathbf{v}}_{u,i}\right).\end{aligned} \tag{31}$$

By setting the first-order error terms in (31), one can obtain the expression

$$\begin{aligned}\sum_{i=2}^{NN_T} t_{u,i1}(\hat{\mathbf{H}}_u^H\hat{\mathbf{H}}_u)\hat{\mathbf{v}}_{u,i} + \mathbf{A}_u\hat{\mathbf{v}}_{u,i} &= x_{u,1}\hat{\mathbf{v}}_{u,i}\\ &+\hat{\lambda}_{u,1}\left(\sum_{i=2}^{NN_T} t_{u,i1}\hat{\mathbf{v}}_{u,i}\right),\end{aligned} \tag{32}$$

which can be further simplified as

$$\sum_{i=2}^{NN_T} t_{u,i1}(\hat{\lambda}_{u,i} - \hat{\lambda}_{u,1})\hat{\mathbf{v}}_{u,i} + \mathbf{A}_u\hat{\mathbf{v}}_{u,1} = x_{u,1}\hat{\mathbf{v}}_{u,1}, \tag{33}$$

Note that $\hat{\mathbf{v}}_{u,1}^T\hat{\mathbf{v}}_{u,i} = 0$, $i \neq 1$, since the eigenvectors corresponding to distinct eigenvalues of a symmetric matrix are orthonormal. Therefore, upon multiplying both sides of (33) with $\hat{\mathbf{v}}_{u,1}^T$, we obtain

$$\begin{aligned}\sum_{i=2}^{NN_T} t_{u,i1}(\hat{\lambda}_{u,i} - \hat{\lambda}_{u,1})\hat{\mathbf{v}}_{u,i}\hat{\mathbf{v}}_{u,j}^T + \mathbf{A}_u\hat{\mathbf{v}}_{u,1}\hat{\mathbf{v}}_{u,i}^T &\\ = x_{u,1}\hat{\mathbf{v}}_{u,1}\hat{\mathbf{v}}_{u,1}^T,&\end{aligned} \tag{34}$$

and the above expression reduces to $t_{u,j1} = \frac{\rho_{u,j1}}{(\hat{\lambda}_{u,1} - \hat{\lambda}_{u,j})}$, where $\rho_{u,ji} = \hat{\mathbf{v}}_{u,j}^T\mathbf{A}_u\hat{\mathbf{v}}_{u,i}$. Substituting the expression for $\rho_{u,ji}$ in (29), with $\epsilon = 1$, which implies that $\mathbf{H}_u^H\mathbf{H}_u = \hat{\mathbf{H}}_u^H\hat{\mathbf{H}}_u + \mathbf{A}_u$ as in (24), the true principal eigenvector $\mathbf{v}_{u,1}$ can be expressed as,

$$\mathbf{v}_{u,1} = \hat{\mathbf{v}}_{u,1} + \sum_{i=2}^{NN_T}\frac{\rho_{u,i1}\hat{\mathbf{v}}_{u,i}}{(\hat{\lambda}_{u,1} - \hat{\lambda}_{u,i})}. \tag{35}$$

Appendix B

Proof of Lemma 2: The magnitude of the perturbation vector $\boldsymbol{\rho}_u$ for the principle eigenvector $\mathbf{v}_{u,1}$ corresponding to the matrix $\mathbf{H}_u^H\mathbf{H}_u$ can be determined using eigenvector perturbation theory [51] as

$$\begin{aligned}\|\boldsymbol{\rho}_u\|_2^2 &= \sum_{j=2}^{NN_T}\left(\frac{1}{\hat{\lambda}_{u,1} - \hat{\lambda}_{u,j}}\right)^2\left\|\hat{\mathbf{v}}_{u,j}^H\mathbf{A}_u\hat{\mathbf{v}}_{u,1}\right\|_2^2\\ &\leq \frac{1}{(\hat{\lambda}_{u,1} - \hat{\lambda}_{u,2})^2}\sum_{j=2}^{NN_T}\left(\hat{\mathbf{v}}_{u,j}^H\mathbf{A}_u\hat{\mathbf{v}}_{u,1}\hat{\mathbf{v}}_{u,1}^H\left(\mathbf{A}_u\right)^H\hat{\mathbf{v}}_{u,j}\right)\\ &\leq \frac{1}{(\hat{\lambda}_{u,1} - \hat{\lambda}_{u,2})^2}\mathrm{Tr}\left(\mathbf{A}_u\hat{\mathbf{v}}_{u,1}\hat{\mathbf{v}}_{u,1}^H\left(\mathbf{A}_u\right)^H\right.\\ &\qquad\left.\times\underbrace{\sum_{j=2}^{NN_T}\hat{\mathbf{v}}_{u,j}\hat{\mathbf{v}}_{u,j}^H + \hat{\mathbf{v}}_{u,1}\hat{\mathbf{v}}_{u,1}^H}_{\sum_{j=1}^{NN_T}\hat{\mathbf{v}}_{u,j}\hat{\mathbf{v}}_{u,j}^H = \mathbf{I}}\right)\\ &\leq \frac{\tilde{\sigma}_u^2}{(\hat{\lambda}_{u,1} - \hat{\lambda}_{u,2})^2}.\end{aligned} \tag{36}$$

Note that the second inequality holds due to the ordered nature of the eigenvalues, i.e., $1/\hat{\lambda}_{u,1} < 1/\hat{\lambda}_{u,2} < \cdots < 1/\hat{\lambda}_{u,NN_T}$. The third inequality follows due to the following facts. First, the quantity $\mathrm{Tr}(\mathbf{A}_u\hat{\mathbf{v}}_{u,1}\hat{\mathbf{v}}_{u,1}^H{\mathbf{A}_u}^H) = \hat{\mathbf{v}}_{u,1}^H{\mathbf{A}_u}^H\mathbf{A}_u\hat{\mathbf{v}}_{u,1}$ is maximum when $\hat{\mathbf{v}}_{u,1}$ is the right singular vector of $\mathbf{A}_u$ corresponding to the largest singular value $\tilde{\sigma}_u$ of the matrix $\mathbf{A}_u$. The maximum value can be determined as the square of the singular value $\tilde{\sigma}_u$.

APPENDIX C

Proof of Theorem 1: Following the framework described in [42], the solution to the SOCP optimization problem in (18) for designing the robust TPC can be obtained as $\tilde{\mathbf{g}}_1^* = -\mu(\mathbf{I}+\mu\mathbf{Q}_1)^{-1}\hat{\mathbf{v}}_{1,1}$, where μ represents the Lagrange multiplier, and the matrix $\mathbf{Q}_1$ is given as

$$\mathbf{Q}_1 = \epsilon_{\rho_1}^2\mathbf{J}_1\mathbf{J}_1^H - \hat{\mathbf{v}}_{1,1}\hat{\mathbf{v}}_{1,1}^H. \tag{37}$$

One can further simplify the expression for $\mathbf{Q}_1$ by substituting the expression for $\mathbf{J}_1$ in (15) as $\mathbf{Q}_1 = \tilde{\mathbf{V}}_1\tilde{\mathbf{\Sigma}}_1\tilde{\mathbf{V}}_1^H$, where the matrices $\tilde{\mathbf{V}}_1$ and $\tilde{\mathbf{\Sigma}}_1$ are defined as

$$\tilde{\mathbf{V}}_1 = [\hat{\mathbf{v}}_{1,1}, \hat{\mathbf{v}}_{1,2}, \ldots, \hat{\mathbf{v}}_{1,NN_T}], \tag{38}$$

$$\tilde{\mathbf{\Sigma}}_1 = \mathrm{diag}\left(-1, \underbrace{\epsilon_{\rho_1}^2, \ldots, \epsilon_{\rho_1}^2}_{NN_T-1 \text{ times}}\right), \tag{39}$$

respectively. Thus, one can employ the properties of the unitary matrix $\hat{\mathbf{V}}_1$ and the eigenvectors to further simplify the TPC vector $\tilde{\mathbf{g}}_1^*$ as

$$\begin{aligned}\tilde{\mathbf{g}}_1^* &= -\mu\Big(\mathbf{I}+\mu\hat{\mathbf{V}}_1\tilde{\mathbf{\Sigma}}_1\hat{\mathbf{V}}_1^{\mathbf{H}}\Big)^{-1}\hat{\mathbf{v}}_{1,1}\\ &= -\mu\Big(\hat{\mathbf{V}}_{\mathbf{1}}^{-\mathbf{1}}\Big)^H(\mathbf{I}+\mu\tilde{\mathbf{\Sigma}}_1)^{-1}\hat{\mathbf{V}}_1^{-1}\hat{\mathbf{v}}_{1,1}\\ &= -\mu\hat{\mathbf{V}}_1(\mathbf{I}+\mu\tilde{\mathbf{\Sigma}}_1)^{-1}\hat{\mathbf{V}}_1^{\mathbf{H}}\hat{\mathbf{v}}_{1,1}\\ &= \frac{\mu}{\mu-1}\hat{\mathbf{v}}_{1,1}.\end{aligned} \tag{40}$$

APPENDIX D

Let the objective function in (22) be represented as

$$f\left(\tilde{\mathbf{F}},\tilde{\sigma}^2\right) = \log\left|\tilde{\mathbf{F}}\tilde{\mathbf{F}}^H + \tilde{\sigma}^2\mathbf{I}_{NN_T}\right|. \tag{41}$$

The Taylor approximation of above function can be written as

$$\begin{aligned}f\left(\tilde{\mathbf{F}},\tilde{\sigma}^2\right) \approx\ & f\left(\tilde{\mathbf{F}}_0,\tilde{\sigma}_0^2\right) + \frac{\partial f\left(\tilde{\mathbf{F}}_0,\tilde{\sigma}_0^2\right)}{\partial\tilde{\sigma}^2}(\tilde{\sigma}^2-\sigma_0^2)\\ &+ \mathrm{Tr}\left\{\left(\frac{\partial f\left(\tilde{\mathbf{F}}_0,\tilde{\sigma}_0^2\right)}{\partial\Re\{\tilde{\mathbf{F}}\}}\right)^T\Re\{\tilde{\mathbf{F}}-\tilde{\mathbf{F}}_0\}\right\}\\ &+ \mathrm{Tr}\left\{\left(\frac{\partial f\left(\tilde{\mathbf{F}}_0,\tilde{\sigma}_0^2\right)}{\partial\Im\{\tilde{\mathbf{F}}\}}\right)^T\Im\{\tilde{\mathbf{F}}-\tilde{\mathbf{F}}_0\}\right\}\end{aligned} \tag{42}$$

One can employ the complex derivative theory [55] to obtain the partial derivatives as

$$\begin{aligned}\frac{\partial f\left(\tilde{\mathbf{F}},\tilde{\sigma}^2\right)}{\partial\Re\{\tilde{\mathbf{F}}\}} &= 2\Re\left\{\frac{\partial f\left(\tilde{\mathbf{F}},\tilde{\sigma}^2\right)}{\partial\tilde{\mathbf{F}}}\right\},\\ \frac{\partial f\left(\tilde{\mathbf{F}},\tilde{\sigma}^2\right)}{\partial\Im\{\tilde{\mathbf{F}}\}} &= 2\Im\left\{\frac{\partial f\left(\tilde{\mathbf{F}},\tilde{\sigma}^2\right)}{\partial\tilde{\mathbf{F}}}\right\}.\end{aligned} \tag{43}$$

Upon substituting (43) in (42), we have

$$\begin{aligned}f\left(\tilde{\mathbf{F}},\tilde{\sigma}^2\right) \approx\ & f\left(\tilde{\mathbf{F}}_0,\tilde{\sigma}_0^2\right) + \frac{\partial f\left(\tilde{\mathbf{F}}_0,\tilde{\sigma}_0^2\right)}{\partial\tilde{\sigma}^2}(\tilde{\sigma}^2-\sigma_0^2)\\ &+ 2\Re\left\{\mathrm{Tr}\left\{\left(\frac{\partial f\left(\tilde{\mathbf{F}}_0,\tilde{\sigma}_0^2\right)}{\partial\Re\{\tilde{\mathbf{F}}\}}\right)^H\Re\left\{\tilde{\mathbf{F}}-\tilde{\mathbf{F}}_0\right\}\right\}\right\}.\end{aligned}$$

For a matrix-valued positive definite differentiable function $\mathbf{L}(x)$, we can write [56]

$$\frac{\log|\mathbf{L}(x)|}{\partial x} = \mathrm{Tr}\left\{\mathbf{L}^{-1}(x)\frac{\partial\mathbf{L}(x)}{\partial x}\right\}. \tag{44}$$

Therefore, the partial derivatives with respect to σ^2 and $\tilde{\mathbf{F}}$ can be written as

$$\begin{aligned}\frac{\partial f\left(\tilde{\mathbf{F}},\tilde{\sigma}^2\right)}{\partial\tilde{\sigma}^2} &= \mathrm{Tr}\left\{\left(\tilde{\mathbf{F}}\tilde{\mathbf{F}}^H+\tilde{\sigma}^2\mathbf{I}_{NN_T}\right)^{-1}\right\},\\ \frac{\partial f\left(\tilde{\mathbf{F}},\tilde{\sigma}^2\right)}{\partial\tilde{\mathbf{F}}^*} &= \left(\tilde{\mathbf{F}}\tilde{\mathbf{F}}^H+\tilde{\sigma}^2\mathbf{I}_{NN_T}\right)^{-1}\tilde{\mathbf{F}}.\end{aligned} \tag{45}$$

Hence, the approximated objective function in (42) can be reformulated as

$$\begin{aligned}f\left(\tilde{\mathbf{F}},\tilde{\sigma}^2\right) \approx\ & f\left(\tilde{\mathbf{F}}_0,\tilde{\sigma}_0^2\right) + \mathrm{Tr}\left\{\mathbf{C}_{y,0}^{-1}\right\}(\tilde{\sigma}^2-\sigma_0^2)\\ &+ 2\Re\left\{\mathrm{Tr}\left\{\tilde{\mathbf{F}}_0^H\mathbf{C}_{y,0}^{-1}\left(\tilde{\mathbf{F}}-\tilde{\mathbf{F}}_0\right)\right\}\right\},\end{aligned} \tag{46}$$

where $\mathbf{C}_{y,0} = \tilde{\mathbf{F}}_0\tilde{\mathbf{F}}_0^H + \tilde{\sigma}_0^2\mathbf{I}_{NN_T}$. We dropped the constant terms from the objective function in the optimization problem. The constraint $\hat{\mathbf{C}}_y \succeq \tilde{\mathbf{F}}\tilde{\mathbf{F}}^H + \tilde{\sigma}^2\mathbf{I}_{NN_T}$ in (22) can be written as [56]

$$\hat{\mathbf{C}}_y \succeq \tilde{\mathbf{F}}\tilde{\mathbf{F}}^H + \tilde{\sigma}^2\mathbf{I}_{NN_T} \Longleftrightarrow \begin{bmatrix}\hat{\mathbf{C}}_y - \tilde{\sigma}^2\mathbf{I}_{NN_T} & \tilde{\mathbf{F}}\\ \tilde{\mathbf{F}}^H & \mathbf{I}_u\end{bmatrix} \succeq 0.$$

REFERENCES

[1] T. S. Rappaport, G. R. MacCartney, M. K. Samimi, and S. Sun, "Wideband millimeter-wave propagation measurements and channel models for future wireless communication system design," *IEEE Transactions on Communications*, vol. 63, no. 9, pp. 3029–3056, 2015.

[2] T. S. Rappaport, S. Sun, R. Mayzus, H. Zhao, Y. Azar, K. Wang, G. N. Wong, J. K. Schulz, M. Samimi, and F. Gutierrez, "Millimeter wave mobile communications for 5G cellular: It will work!" *IEEE access*, vol. 1, pp. 335–349, 2013.

[3] I. A. Hemadeh, K. Satyanarayana, M. El-Hajjar, and L. Hanzo, "Millimeter-wave communications: Physical channel models, design considerations, antenna constructions, and link-budget," *IEEE Communications Surveys & Tutorials*, vol. 20, no. 2, pp. 870–913, 2017.

[4] A. Moerman, J. Van Kerrebrouck, O. Caytan, I. L. de Paula, L. Bogaert, G. Torfs, P. Demeester, H. Rogier, and S. Lemey, "Beyond 5G without obstacles: mmWave-over-fiber distributed antenna systems," *IEEE Communications Magazine*, vol. 60, no. 1, pp. 27–33, 2022.

[5] M. B. Majed, T. A. Rahman, and O. A. Aziz, "Propagation path loss modeling and outdoor coverage measurements review in millimeter wave bands for 5G cellular communications," *International Journal of Electrical and Computer Engineering*, vol. 8, no. 4, p. 2254, 2018.

[6] M. Jafri, A. Anand, S. Srivastava, A. K. Jagannatham, and L. Hanzo, "Robust distributed hybrid beamforming in coordinated multi-user multi-cell mmWave MIMO systems relying on imperfect CSI," *IEEE Transactions on Communications*, vol. 70, no. 12, pp. 8123–8137, 2022.

[7] C. Pan, M. Elkashlan, J. Wang, J. Yuan, and L. Hanzo, "User-centric C-RAN architecture for ultra-dense 5G networks: Challenges and methodologies," *IEEE Communications Magazine*, vol. 56, no. 6, pp. 14–20, 2018.

[8] G. Femenias and F. Riera-Palou, "Cell-free millimeter-wave massive MIMO systems with limited fronthaul capacity," *IEEE Access*, vol. 7, pp. 44 596–44 612, 2019.

[9] Q. Li, M. El-Hajjar, C. Xu, J. An, C. Yuen, and L. Hanzo, "Stacked intelligent metasurfaces for holographic MIMO aided cell-free networks," *IEEE Transactions on Communications*, 2024.

[10] Z. Mobini, H. Q. Ngo, M. Matthaiou, and L. Hanzo, "Cell-free massive MIMO surveillance of multiple untrusted communication links," *IEEE Internet of Things Journal*, 2024.

[11] S. Rangan, T. S. Rappaport, and E. Erkip, "Millimeter-wave cellular wireless networks: Potentials and challenges," *Proceedings of the IEEE*, vol. 102, no. 3, pp. 366–385, 2014.

[12] L. Wei, R. Q. Hu, Y. Qian, and G. Wu, "Key elements to enable millimeter wave communications for 5G wireless systems," *IEEE Wireless Communications*, vol. 21, no. 6, pp. 136–143, 2014.

[13] S. Kutty and D. Sen, "Beamforming for millimeter wave communications: An inclusive survey," *IEEE Communications Surveys & Tutorials*, vol. 18, no. 2, pp. 949–973, 2015.

[14] R. W. Heath, N. Gonzalez-Prelcic, S. Rangan, W. Roh, and A. M. Sayeed, "An overview of signal processing techniques for millimeter wave MIMO systems," *IEEE Journal of Selected Topics in Signal Processing*, vol. 10, no. 3, pp. 436–453, 2016.

[15] O. El Ayach, S. Rajagopal, S. Abu-Surra, Z. Pi, and R. W. Heath, "Spatially sparse precoding in millimeter wave MIMO systems," *IEEE Transactions on Wireless Communications*, vol. 13, no. 3, pp. 1499–1513, 2014.

[16] Q. Yue, J. Hu, T. Shui, Q. Huang, K. Yang, and L. Hanzo, "Hybrid terahertz beamforming relying on channel sparsity and angular orthogonality," *IEEE Transactions on Vehicular Technology*, 2023.

[17] A. Alkhateeb, J. Mo, N. Gonzalez-Prelcic, and R. W. Heath, "MIMO precoding and combining solutions for millimeter-wave systems," *IEEE Communications Magazine*, vol. 52, no. 12, pp. 122–131, 2014.

[18] X. Yu, J.-C. Shen, J. Zhang, and K. B. Letaief, "Alternating minimization algorithms for hybrid precoding in millimeter wave MIMO systems," *IEEE Journal of Selected Topics in Signal Processing*, vol. 10, no. 3, pp. 485–500, 2016.

[19] S. S. Ioushua and Y. C. Eldar, "A family of hybrid analog-digital beamforming methods for massive MIMO systems," *IEEE Transactions on Signal Processing*, vol. 67, no. 12, pp. 3243–3257, 2019.

[20] C. G. Tsinos, S. Maleki, S. Chatzinotas, and B. Ottersten, "On the energy-efficiency of hybrid analog-digital transceivers for single-and multi-carrier large antenna array systems," *IEEE Journal on Selected Areas in Communications*, vol. 35, no. 9, pp. 1980–1995, 2017.

[21] L. Liang, W. Xu, and X. Dong, "Low-complexity hybrid precoding in massive multiuser MIMO systems," *IEEE Wireless Communications Letters*, vol. 3, no. 6, pp. 653–656, 2014.

[22] W. Ni and X. Dong, "Hybrid block diagonalization for massive multiuser MIMO systems," *IEEE Transactions on Communications*, vol. 64, no. 1, pp. 201–211, 2015.

[23] A. Alkhateeb, G. Leus, and R. W. Heath, "Limited feedback hybrid precoding for multi-user millimeter wave systems," *IEEE Transactions on Wireless Communications*, vol. 14, no. 11, pp. 6481–6494, 2015.

[24] F. Sohrabi and W. Yu, "Hybrid digital and analog beamforming design for large-scale antenna arrays," *IEEE Journal of Selected Topics in Signal Processing*, vol. 10, no. 3, pp. 501–513, 2016.

[25] J. Zhan and X. Dong, "Interference cancellation aided hybrid beamforming for mmWave multi-user massive MIMO systems," *IEEE Transactions on Vehicular Technology*, vol. 70, no. 3, pp. 2322–2336, 2021.

[26] G. Zhu, K. Huang, V. K. Lau, B. Xia, X. Li, and S. Zhang, "Hybrid beamforming via the kronecker decomposition for the millimeter-wave massive MIMO systems," *IEEE Journal on Selected Areas in Communications*, vol. 35, no. 9, pp. 2097–2114, 2017.

[27] S. Sun, T. S. Rappaport, M. Shafi, and H. Tataria, "Analytical framework of hybrid beamforming in multi-cell millimeter-wave systems," *IEEE Transactions on Wireless Communications*, vol. 17, no. 11, pp. 7528–7543, 2018.

[28] J. Kim, S.-H. Park, O. Simeone, I. Lee, and S. S. Shitz, "Joint design of fronthauling and hybrid beamforming for downlink C-RAN systems," *IEEE Transactions on Communications*, vol. 67, no. 6, pp. 4423–4434, 2019.

[29] C. Fang, B. Makki, J. Li, and T. Svensson, "Hybrid precoding in cooperative millimeter wave networks," *IEEE Transactions on Wireless Communications*, vol. 20, no. 8, pp. 5373–5388, 2021.

[30] M. Alonzo, S. Buzzi, A. Zappone, and C. D'Elia, "Energy-efficient power control in cell-free and user-centric massive MIMO at millimeter wave," *IEEE Transactions on Green Communications and Networking*, vol. 3, no. 3, pp. 651–663, 2019.

[31] C. Feng, W. Shen, J. An, and L. Hanzo, "Weighted sum rate maximization of the mmWave cell-free MIMO downlink relying on hybrid precoding," *IEEE Transactions on Wireless Communications*, vol. 21, no. 4, pp. 2547–2560, 2021.

[32] N. T. Nguyen, K. Lee, and H. Dai, "Hybrid beamforming and adaptive RF chain activation for uplink cell-free millimeter-wave massive MIMO systems," *IEEE Transactions on Vehicular Technology*, vol. 71, no. 8, pp. 8739–8755, 2022.

[33] M. Jafri, S. Srivastava, N. K. D. Venkategowda, A. K. Jagannatham, and L. Hanzo, "Cooperative hybrid transmit beamforming in cell-free mmWave MIMO networks," *IEEE Transactions on Vehicular Technology*, vol. 72, no. 5, pp. 6023–6038, 2023.

[34] Q. Peng, H. Ren, M. Dong, M. Elkashlan, K.-K. Wong, and L. Hanzo, "Resource allocation for cell-free massive MIMO-aided URLLC systems relying on pilot sharing," *IEEE Journal on Selected Areas in Communications*, vol. 41, no. 7, pp. 2193–2207, 2023.

[35] T. Zhao, S. Chen, R. Zhang, H.-H. Chen, and Q. Guo, "Uplink channel estimation with reduced fronthaul overhead in cell-free massive MIMO systems," *IEEE Wireless Communications Letters*, vol. 11, no. 8, pp. 1718–1722, 2022.

[36] G. Zheng, K.-K. Wong, and B. Ottersten, "Robust cognitive beamforming with bounded channel uncertainties," *IEEE Transactions on Signal Processing*, vol. 57, no. 12, pp. 4871–4881, 2009.

[37] V. M. Palhares, A. R. Flores, and R. C. De Lamare, "Robust MMSE precoding and power allocation for cell-free massive MIMO systems," *IEEE Transactions on Vehicular Technology*, vol. 70, no. 5, pp. 5115–5120, 2021.

[38] N. Li, J. Jin, L. Xia, Q. Wang, G. Liu, Z. Chen, and Z. Hu, "Robust low complexity beamforming for cell-free massive MIMO," in *2020 IEEE 92nd Vehicular Technology Conference (VTC2020-Fall)*. IEEE, 2020, pp. 1–5.

[39] D. Yu, S.-H. Park, O. Simeone, and S. S. Shitz, "Robust design of rate-splitting multiple access with imperfect CSI for cell-free MIMO systems," in *2022 IEEE International Conference on Communications Workshops (ICC Workshops)*. IEEE, 2022, pp. 604–609.

[40] J. Yao, J. Xu, W. Xu, D. W. K. Ng, C. Yuen, and X. You, "Robust beamforming design for RIS-aided cell-free systems with CSI uncertainties and capacity-limited backhaul," *IEEE Transactions on Communications*, 2023.

[41] T. S. Rappaport, R. W. Heath Jr, R. C. Daniels, and J. N. Murdock, *Millimeter wave wireless communications*. Pearson Education, 2015.

[42] R. G. Lorenz and S. P. Boyd, "Robust minimum variance beamforming," *IEEE Transactions on Signal Processing*, vol. 53, no. 5, pp. 1684–1696, 2005.

[43] J. Li, P. Stoica, and Z. Wang, "On robust Capon beamforming and diagonal loading," *IEEE Transactions on Signal Processing*, vol. 51, no. 7, pp. 1702–1715, 2003.

[44] R. Wang, H. Li, and T. Li, "Robust multiuser detection for multicarrier CDMA systems," *IEEE Journal on Selected Areas in Communications*, vol. 24, no. 3, pp. 673–683, 2006.

[45] M. Grant and S. Boyd, "CVX: MATLAB software for disciplined convex programming, version 2.1," 2014.

[46] L. Liu, R. Chen, S. Geirhofer, K. Sayana, Z. Shi, and Y. Zhou, "Downlink MIMO in LTE-advanced: SU-MIMO vs. MU-MIMO," *IEEE Communications Magazine*, vol. 50, no. 2, pp. 140–147, 2012.

[47] S. Kim and B. Shim, "Energy-efficient millimeter-wave cell-free systems under limited feedback," *IEEE Transactions on Communications*, vol. 69, no. 6, pp. 4067–4082, 2021.

[48] C. Zhang, P. Du, M. Ding, Y. Jing, and Y. Huang, "Joint port selection based channel acquisition for FDD cell-free massive MIMO," *IEEE Transactions on Communications*, 2024.

[49] Y. Jin, J. Zhang, S. Jin, and B. Ai, "Channel estimation for cell-free mmwave massive MIMO through deep learning," *IEEE Transactions on Vehicular Technology*, vol. 68, no. 10, pp. 10 325–10 329, Oct 2019.

[50] H. Song, T. Goldstein, X. You, C. Zhang, O. Tirkkonen, and C. Studer, "Joint channel estimation and data detection in cell-free massive MU-MIMO systems," *IEEE Transactions on Wireless Communications*, 2021.

[51] J. H. Wilkinson, *The algebraic eigenvalue problem*. Oxford University Press, Inc., 1988.

[52] M. Rubsamen and A. B. Gershman, "Robust adaptive beamforming using multidimensional covariance fitting," *IEEE Transactions on Signal Processing*, vol. 60, no. 2, pp. 740–753, 2011.

[53] B. Liu, Y. Cheng, and Q. Zhou, "Robust rank-two beamforming for multicell multigroup multicast," *IET Communications*, vol. 10, no. 3, pp. 283–291, 2016.

[54] G.-W. Hsu, B. Liu, H.-H. Wang, and H.-J. Su, "Joint beamforming for multicell multigroup multicast with per-cell power constraints," *IEEE Transactions on Vehicular Technology*, vol. 66, no. 5, pp. 4044–4058, 2016.

[55] D. H. Brandwood, "A complex gradient operator and its application in adaptive array theory," in *IEE Proceedings H (Microwaves, Optics and Antennas)*, vol. 130, no. 1. IET Digital Library, 1983, pp. 11–16.

[56] H. L. Van Trees, *Optimum array processing: Part IV of detection, estimation, and modulation theory*. John Wiley & Sons, 2002.